Life Sciences in Space Research 9 (2016) 69–76

Contents lists available at ScienceDirect

Life Sciences in Space Research

journal homepage: www.elsevier.com/locate/lssr

Solar proton exposure of an ICRU sphere within a complex structure Part I: Combinatorial geometry

John W. Wilson[a], Tony C. Slaba[b,*], Francis F. Badavi[a], Brandon D. Reddell[c], Amir A. Bahadori[c]

[a] Old Dominion University, Norfolk VA 23529 USA
[b] NASA Langley Research Center, Hampton VA 23681-2199 USA
[c] NASA Johnson Space Center, Houston, TX 77004 USA

ARTICLE INFO

Article history:
Received 16 February 2016
Revised 29 April 2016
Accepted 9 May 2016

Keywords:
Space radiation
Radiation shielding
Radiation transport
HZETRN

ABSTRACT

The 3DHZETRN code, with improved neutron and light ion ($Z \leq 2$) transport procedures, was recently developed and compared to Monte Carlo (MC) simulations using simplified spherical geometries. It was shown that 3DHZETRN agrees with the MC codes to the extent they agree with each other. In the present report, the 3DHZETRN code is extended to enable analysis in general combinatorial geometry. A more complex shielding structure with internal parts surrounding a tissue sphere is considered and compared against MC simulations. It is shown that even in the more complex geometry, 3DHZETRN agrees well with the MC codes and maintains a high degree of computational efficiency.

Published by Elsevier Ltd on behalf of The Committee on Space Research (COSPAR).

1. Introduction

A three dimensional (3D) version of HZETRN has recently been developed and tested in simple geometries and compared to available Monte Carlo (MC) codes (Wilson et al. 2014a–c, 2015a). In the first study (Wilson et al. 2014a, b), an aluminum sphere with a radial thickness of 20 g/cm^2 was examined, and comparisons were made between 3DHZETRN results and MC simulations at locations within the sphere exposed to solar particle event (SPE) and galactic cosmic ray (GCR) boundary conditions. Well defined convergence tests were performed that spanned the transport formalism, covering the straight ahead approximation ($N = 1$), bi-directional approximation ($N = 2$), and more detailed 3D treatment ($N > 2$) for neutrons and light ions. Note that in the formalism of Wilson et al. (2014a–c, 2015a), N denotes the number of transport directions used to describe the assumed isotropic neutron and light ion fluxes at lower energies. The convergence tests and comparison to MC results established improved description of the neutron and light ion solutions within the 3D formalism. It was also shown that although there are still noticeable differences associated with the nuclear production models used in the codes, 3DHZETRN agreed with the MC models to the extent they agree with each other in finite geometry. The main difference between the transport codes was found to be in the computational costs. While 3DHZETRN results were generated in several seconds on a single CPU, the MC code run times were several orders of magnitude larger ($\sim 10^8$ s) and required high performance computing clusters.

In the next study (Wilson et al. 2014c, 2015a), a tissue sphere with a radial thickness of 15 g/cm^2, defined by the International Commission on Radiation Units and Measurements (ICRU) (ICRU 1993), was surrounded by an aluminum spherical shell with thickness 20 g/cm^2, and similar convergence tests and comparisons to MC were provided. Improvements in the low energy neutron and light ion spectra as a result of 3D corrections were again clearly established. Despite the added geometric complexity of the two material sphere configuration, agreement between all the codes was actually improved compared to the previous single material aluminum sphere. The improved agreement was attributed to the hydrogen content of the ICRU tissue sphere. For energies below ~100 MeV, elastic collisions between neutrons and hydrogen dominate the neutron transport processes. These elastic collisions, on average, transfer half the neutron energy to the target hydrogen, which in turn, very rapidly attenuates the neutron energy spectrum. Although neutron production cross sections show significant variation amongst the codes for aluminum targets, as seen in the first study (Wilson et al. 2014a, b), neutron-hydrogen elastic cross sections are more precisely and accurately represented in the codes either through evaluated nuclear data files or detailed parameterizations (Wilson et al. 1991). Again, it was found that 3DHZETRN was in good agreement with the MC simulation results, and the primary difference between the codes lay in the associated computational costs, where 3DHZETRN is several orders of magnitude faster.

* Corresponding author. Tel.: +1 757 864 1420.
E-mail address: tony.c.slaba@nasa.gov (T.C. Slaba).

http://dx.doi.org/10.1016/j.lssr.2016.05.002
2214-5524/Published by Elsevier Ltd on behalf of The Committee on Space Research (COSPAR).

Herein, a more complex and realistic shielding geometry with multiple parts is considered (Wilson et al. 2015b). An ICRU tissue sphere is surrounded by a cylindrical aluminum shell containing two additional internal aluminum boxes. The sizes and locations of the internal boxes are chosen to provide partial shielding of the ICRU sphere, thereby emphasizing 3D effects in the transport process. The chosen geometry is sufficiently complex to further test 3DHZETRN while still allowing engagement of various MC codes to verify the solution methods.

In this report, transport code development efforts will be briefly reviewed with an emphasis on the most recent extensions leading to a generalized version of 3DHZETRN applicable in combinatorial geometry. As in the previous studies (Wilson et al. 2014a–c, 2015a), convergence tests are performed and comparison to MC simulations are provided. The next step in 3DHZETRN development will allow the use of more complex and realistic geometric models, including human phantoms, so that simple mapping of the present methodology into more realistic applications can be studied. Although a final solution to engineering design problems is not yet at hand, the current status of deterministic methods agrees with MC codes to the degree that various MC codes agree among themselves in many cases. The main limitation within 3DHZETRN remains in the nuclear databases and requires additional experimental measurements and nuclear model development.

2. 3DHZETRN

The 3DHZETRN theoretical formalism has been provided in prior reports (Wilson et al. 2014a–c, 2015a) and will not be repeated in detail here. However, an overview is given here to provide clarity in the notation and terminology used later in this paper. Additional discussion is given in this section regarding extensions of the present code to general combinatorial geometry.

2.1. Theoretical formalism overview

The linear Boltzmann transport equation within the continuous slowing down approximation for the flux (or fluence) density, $\phi_j(\boldsymbol{x}, \boldsymbol{\Omega}, E)$, of a j type particle is given by (Wilson et al. 1991, 2005)

$$\mathbf{B}[\phi_j(\boldsymbol{x}, \boldsymbol{\Omega}, E)] = \sum_k \int_E^\infty \int_{4\pi} \sigma_{jk}(E, E', \boldsymbol{\Omega}, \boldsymbol{\Omega}')\phi_k(\boldsymbol{x}, \boldsymbol{\Omega}', E')\, d\boldsymbol{\Omega}'\, dE', \tag{1}$$

where the differential operator on the left hand side is defined as

$$\mathbf{B}[\phi_j(\boldsymbol{x}, \boldsymbol{\Omega}, E)] \equiv \boldsymbol{\Omega} \cdot \nabla\phi_j(\boldsymbol{x}, \boldsymbol{\Omega}, E) - \frac{1}{A_j}\frac{\partial}{\partial E}\left[S_j(E)\phi_j(\boldsymbol{x}, \boldsymbol{\Omega}, E)\right] + \sigma_j(E)\phi_j(\boldsymbol{x}, \boldsymbol{\Omega}, E). \tag{2}$$

In Eqs. (1) and (2), A_j is the atomic mass of a type j particle, $S_j(E)$ is the stopping power of a type j ion with kinetic energy E (which vanishes for neutrons), $\sigma_j(E)$ is the total macroscopic cross section for a type j particle with kinetic energy E, and $\sigma_{jk}(E, E', \boldsymbol{\Omega}, \boldsymbol{\Omega}')$ is the double differential macroscopic production cross section for interactions in which a type k particle with kinetic energy E' and direction $\boldsymbol{\Omega}'$ produce a type j particle with kinetic energy E and direction $\boldsymbol{\Omega}$.

Solution methods are developed by separating the double differential cross section for neutron ($j = n$) production and the particle fluxes into forward and isotropic components. The forward components are associated mainly with higher energy direct quasi-elastic events and projectile fragmentation products (Wilson 1977; Wilson et al. 1988), and the isotropic components are associated with lower energy secondary particles, including target fragments.

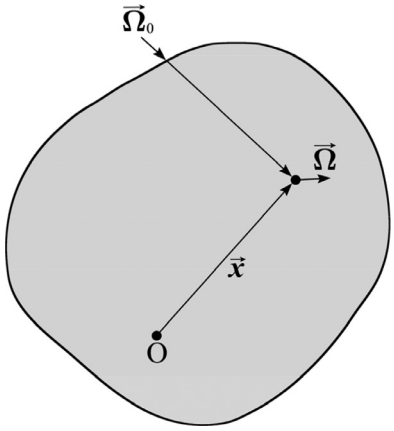

Fig. 1. Geometry depicting relationship between the forward direction Ω_0 and transport direction Ω at location x.

The forward component is first solved within the straight ahead approximation, wherein all particles are assumed to travel along a common axis ($\boldsymbol{\Omega} \approx \boldsymbol{\Omega}'$). This allows previously developed and highly efficient numerical solution techniques to be utilized (Wilson et al. 1991; Slaba et al. 2010a). The forward solution then gives rise to a source of isotropically produced neutrons, given as

$$\xi_{n,iso}(\boldsymbol{x}, \boldsymbol{\Omega}, \boldsymbol{\Omega}_0, E) = \sum_k \int_E^\infty \sigma_{nk,iso}(E, E', \boldsymbol{\Omega}, \boldsymbol{\Omega}_0)\phi_{k,for}(\boldsymbol{x}, \boldsymbol{\Omega}_0, E')\, dE', \tag{3}$$

where $\sigma_{nk,iso}(E,E',\boldsymbol{\Omega},\boldsymbol{\Omega}')$ is the isotropic component of the neutron production cross section, and $\phi_{k,for}(\boldsymbol{x},\boldsymbol{\Omega},E')$ is the forward component of the flux. The symbol $\boldsymbol{\Omega}_0$ denotes the direction of the inbound forward flux arriving at location $\boldsymbol{x}$, and $\boldsymbol{\Omega}$ denotes the transport direction within the geometry along which the isotropic flux is being computed, as in Fig. 1. The transport equation for the isotropic neutron flux is given by

$$[\boldsymbol{\Omega} \cdot \nabla + \sigma_n(E)]\phi_{n,iso}(\boldsymbol{x}, \boldsymbol{\Omega}, E) = \int_E^\infty \int_{4\pi} \sigma_{nn}(E, E', \boldsymbol{\Omega}, \boldsymbol{\Omega}')\phi_{n,iso}(\boldsymbol{x}, \boldsymbol{\Omega}', E')\, d\boldsymbol{\Omega}'\, dE' + \xi_{n,iso}(\boldsymbol{x}, \boldsymbol{\Omega}, \boldsymbol{\Omega}_0, E). \tag{4}$$

Eq. (4) is solved along the transport direction $\boldsymbol{\Omega}$ within the bi-directional approximation discussed in detail elsewhere (Slaba et al. 2010b). A final step in the solution methodology is to compute the source of light ions produced from the lower energy isotropic neutrons. Once this source is computed, the isotropic component of the light ion flux is solved under the assumption that no further nuclear collisions occur, giving partial 3D treatment to low energy charged particles.

A remaining detail in the transport formalism is to define a discrete number, N, of transport directions, $\boldsymbol{\Omega}$, over which the isotropic flux is evaluated. In connecting to historical code development, the $N = 1$ solution corresponds to the usual straight ahead approximation wherein all particles are assumed to follow a common axis. In this case, there is only one transport direction $\boldsymbol{\Omega}$, and $\boldsymbol{\Omega} = \boldsymbol{\Omega}_0$. The $N = 2$ solution corresponds to the bi-directional transport approximation, wherein particles are allowed to propagate either straight forward or straight backward. In this case, there are two transport directions ($\boldsymbol{\Omega}_1 = \boldsymbol{\Omega}_0$ and $\boldsymbol{\Omega}_2 = -\boldsymbol{\Omega}_0$). Values of $N > 2$, correspond to a more detailed three dimensional (3D) description of the isotropic flux component and are the emphasis of recent advances in code development (Wilson et al. 2014a–c, 2015a). In those previous studies, values of $N = 1, 2, 6, 10, 14, 18, 22$ were considered, as shown in Fig. 2.